catalysts

MDPI

Article

Solar-Driven Removal of 1,4-Dioxane Using $WO_3/n\gamma\text{-}Al_2O_3$ Nano-catalyst in Water

Xiyan Xu [1], Shuming Liu [1,*], Yong Cui [2], Xiaoting Wang [1], Kate Smith [1] and Yujue Wang [1]

1 School of Environment, Tsinghua University, Beijing 100084, China; xiyanxu@tsinghua.edu.cn (X.X.); wang-xt15@mails.tsinghua.edu.cn (X.W.); skt15@mails.tsinghua.edu.cn (K.S.); wangyujue@tsinghua.edu.cn (Y.W.)

2 Boda Water Co., Ltd., Beijing 100176, China; cuiyong@bdawater.com

* Correspondence: shumingliu@tsinghua.edu.cn; Tel./Fax: +86-10-6278-7964

Received: 5 April 2019; Accepted: 24 April 2019; Published: 25 April 2019

Abstract: Increasing demand for fresh water in extreme drought regions necessitates potable water reuse. However, current membrane-based water reclamation approaches cannot effectively remove carcinogenic 1,4-dioxane. The current study reports on the solar-driven removal of 1,4-dioxane (50 mg L^{-1}) using a homemade $WO_3/n\gamma\text{-}Al_2O_3$ nano-catalyst. Characterization methods including scanning electron microscope (SEM), X-ray photoelectron spectroscopy (XPS) and X-ray fluorescence (XRF) analyses are used to investigate the surface features of the catalyst. The 1,4-dioxane mineralization performance of this catalyst under various reaction conditions is studied. The effect of the catalyst dosage is tested. The mean oxidation state carbon (MOSC) values of the 1,4-dioxane solution are followed during the reaction. The short chain organic acids after treatment are measured. The results showed that over 75% total organic carbon (TOC) removal was achieved in the presence of 300 mg L^{-1} of the catalyst with a simulated solar irradiation intensity of 40 mW cm^{-2}. Increasing the dose of the catalyst from 100 to 700 mg L^{-1} can improve the treatment efficiency to some extent. The TOC reduction curve fits well with an apparent zero-order kinetic model and the corresponding constant rates are within 0.0927 and 0.1059 mg L^{-1} s^{-1}, respectively. The MOSC values of the 1,4-dioxane solution increase from 1.3 to 3 along the reaction, which is associated with the formation of some short chain acids. The catalyst can be effectively reused 7 times. This work provides an oxidant-free and energy saving approach to achieve efficient removal of 1,4-dioxane and thus shows promising potential for potable reuse applications.

Keywords: 1,4-dioxane; photocatalysis; $WO_3/n\gamma\text{-}Al_2O_3$; solar radiation; water treatment; potable reuse

1. Introduction

Rapid population expansion of cities results in increasing water consumption and requires exploitation of alternative water resources for potable purposes, especially in extremely water-scarce regions [1–4]. Membrane-based water purification techniques including ultrafiltration (UF) and reverse osmosis (RO) can effectively remove the major proportion of salts and organic contaminants in municipal wastewater secondary effluent (MWSE) [5–9]. However, some micropollutants including 1,4-dioxane (1,4-D) present in the MWSE in trace concentrations cannot be easily removed [10]. 1,4-D is a reagent stabilizer in industrial chlorinated solvents, which commonly exists in cosmetics, toiletries, and food addictive [11–13]. Uncontrolled exposure to 1,4-D can cause failures of human organs including kidney and liver [14,15]. It can even cause cancer when it exists in drinking water. Thus, it has been classified as a Group 2B human carcinogen [1].

Therefore, 1,4-D should be eliminated if the reclamation of MWSE for potable reuse is required [10]. Advanced oxidation processes (AOPs) have been extensively applied to decompose or even mineralize organic pollutants in water [8,16–21]. Reactive free radicals, or more specifically reactive oxygen species (ROS) like $HO^{\bullet}$ and $HO_2^{\bullet}/O^{\bullet-}$, can be formed from the activation of oxidants by reagents or energy in these systems. These ROS tend to attack organic pollutants and result in their degradation [22–26]. Photolytic AOPs can take advantage of the photons' energy, especially ultraviolet (UV), to activate the oxidants [27]. In order to eliminate 1,4-D from water for potable reuse, recent studies provided several possible solutions based on photolytic AOP approaches [1,28,29]. Patton et al. investigated the performance of UV/H_2O_2-based system for 1,4-D removal in the presence of mono- and dichloramines [1]. On that basis, Li et al. used another oxidant (persulfate, $S_2O_8^{2-}$) to establish a UV/$S_2O_8^{2-}$ system to eliminate 1,4-D [5]. Although these works revealed that mono- or dichloramines can promote treatment efficiency to some extent by participating in the reaction processes, these systems inevitably introduce external reagents (the oxidants) into the target solution. This compromises the practical application of those methods for potable water reuse since the effect of the residual reagents on human health needs to be further considered.

Photocatalytic oxidation systems are possible candidates to avoid that drawback. In photocatalytic systems, oxidants are not indispensable since ROS can be formed from the activation of dissolved oxygen or even water molecules by the photocatalysts under photoirradiation [30–32]. Electrons on the valence band (VB) of the catalyst can be excited to transit to the conduction band (CB) when the energy of photoirradiation reaches the band gap [33]. Electron/hole (h^+/e^-) pairs can be formed on the catalysts during this process and lead to formation of ROS from dissolved oxygen and water molecules [30,34]. Photocatalytic approaches have been used to treat 1,4-D contaminated water [35–37]. However, these systems were mainly activated by UV light rather than visible light, since the band gap of traditional photocatalysts (like TiO_2) is so broad that photons with lower energy (visible light) are not capable of inducing the formation of ROS [38,39].

Tungsten-based catalysts have been developed in recent years since they are sensitive to visible light and thus can improve the photocatalytic efficiency [40–43]. Meanwhile, γ-Al_2O_3 supporter showed more desirable stability in AOP systems than conventional supporters like activated carbon due to its high active phase-supporter interaction [16]. Moreover, using nano-size supporters may provide a stronger active phase-supporter link due to their unique features like extremely large specific surface area. Thus, the nano-size supporters have the potential to improve the reusability of the catalyst [44]. However, to the best of our knowledge, no previous study applied nano tungsten-based catalysts with γ-Al_2O_3 as the supporter for the photocatalytic breakdown of 1,4-D.

The current study aimed at the removal of 1,4-D using an oxidant-free photocatalytic system with a homemade nano-size tungsten-based catalyst (WO_3/nγ-Al_2O_3) under solar light irradiation. The characteristics of the catalyst were studied using scanning electron microscope (SEM), X-ray photoelectron spectroscopy (XPS) and X-ray fluorescence (XRF). 1,4-D mineralization efficiency under various conditions was considered and the reaction kinetic rates were calculated. The effect of the catalyst dosage was tested. The oxidation state of the effluent solution during the reaction was followed and the formation of short chain organic acids after the reaction was measured.

2. Results and Discussion

2.1. Characterization of the Catalyst

To have an insight into the features of the WO_3/nγ-Al_2O_3 catalyst, characterization was conducted. The SEM image (Figure 1a) shows the appearance of the prepared catalyst. It can be seen that the shape of the catalyst is roughly sphere-like.

The diameter of the catalyst is around 50 nm (Figure 1a). XPS analyses of the WO_3/nγ-Al_2O_3 catalyst were also conducted. Figure 1b depicts the W 4f core level XPS spectra. There are two symmetric peaks at binding energies 35.9 and 37.4 eV, which are associated with the W-Al band and

WO_3, respectively [45,46]. The O 1s XPS profile (Figure 1c) shows two symmetric peaks at 530.8 and 532.7 eV. These two peaks correspond to WO_3 and Al_2O_3, respectively [47,48]. Al 2p XPS spectra profile (Figure 1d) shows two peaks at 74.5 and 75.9 eV, which are associated to the Al-W band and Al_2O_3 [45,49], respectively. The XPS spectra profiles support the fact that a certain amount of active phase (WO_3) has been loaded on the carrier (nγ-Al_2O_3). It can be inferred from the results that the three elements (W, O, and Al) are interconnected in terms of WO_3 and Al_2O_3 and the former two compounds are probably connected by the W-Al band.

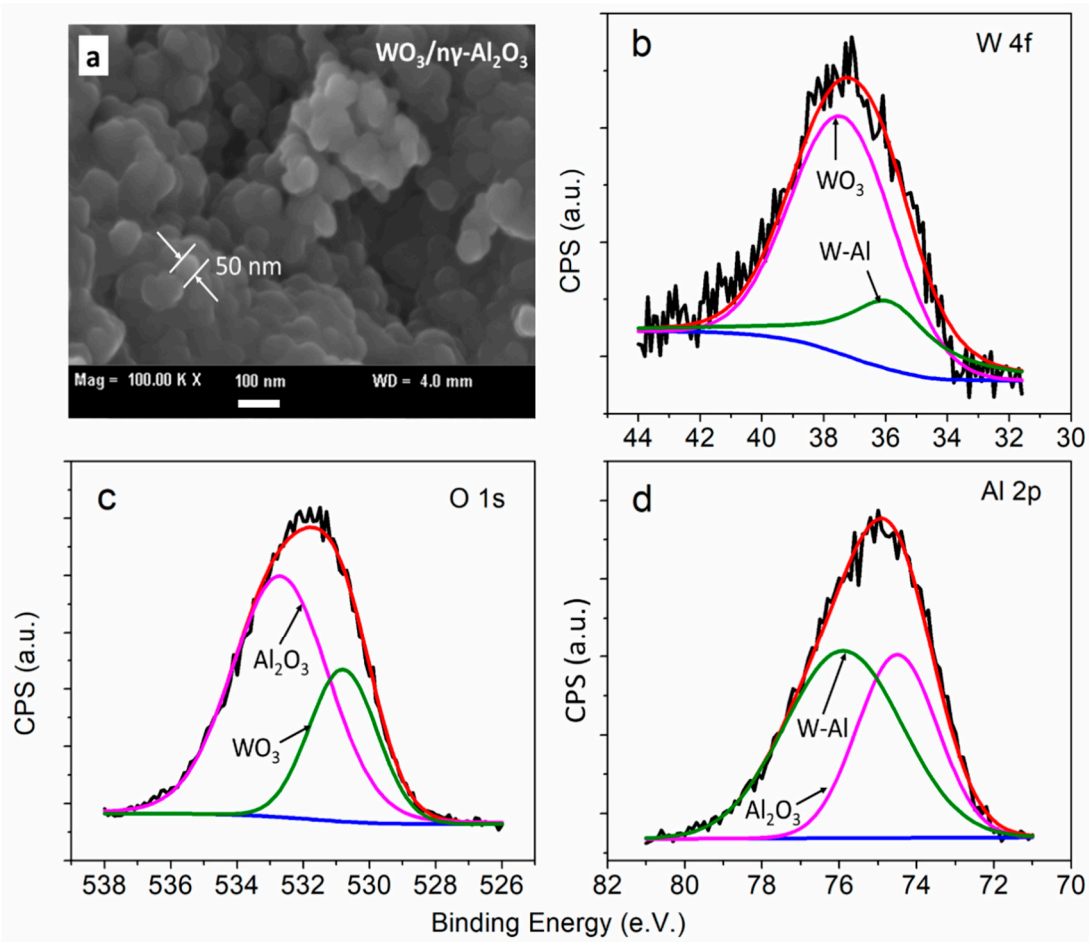

Figure 1. (**a**) SEM image and (**b**) W 4f, (**c**) O 1s and (**d**) Al 2p core level X-ray photoelectron spectroscopy (XPS) spectra of the WO_3/nγ-Al_2O_3 catalyst.

XRF profile provides quantitative proportions of the surface compounds on the catalyst (Table 1) where the weight percentage of WO_3 is 4.73% on the catalyst surface, confirming that WO_3 was formed and fixed on the surface of the catalysts.

Table 1. Percentages of surface compounds on the WO_3/nγ-Al_2O_3 catalyst from X-ray fluorescence (XRF).

Compound	Wt (%) *	Error
Al_2O_3	94.15	0.12
WO_3	4.73	0.11
Others	1.12	–

* Wt (%), the weight percent.

2.2. Solar-Driven Removal of 1,4-D

Solar-driven oxidation of 1,4-D was firstly conducted without the catalyst. As can be seen in Figure 2a, less than 17% of mineralization can be achieved after 4 h. This limited removal is due to the non-photosensitive structure of 1,4-D [15,36]. A comparative experiment using the catalyst in dark conditions was also carried out to check the contribution of adsorption for 1,4-D removal. Figure 2a shows that almost no total organic carbon (TOC) removal can be observed under these conditions, indicating the negligible effect of adsorption. Then, 1,4-D was exposed under solar radiation in the presence of the $WO_3/n\gamma\text{-}Al_2O_3$ nano-catalyst. Under this condition, a significant TOC reduction (over 75%) was obtained following a reaction time of 4 h Figure 2a. The above results indicate that the current $WO_3/n\gamma\text{-}Al_2O_3$ nano-catalyst can effectively mineralize 1,4-D and the effect is mainly due to photocatalytic decomposition.

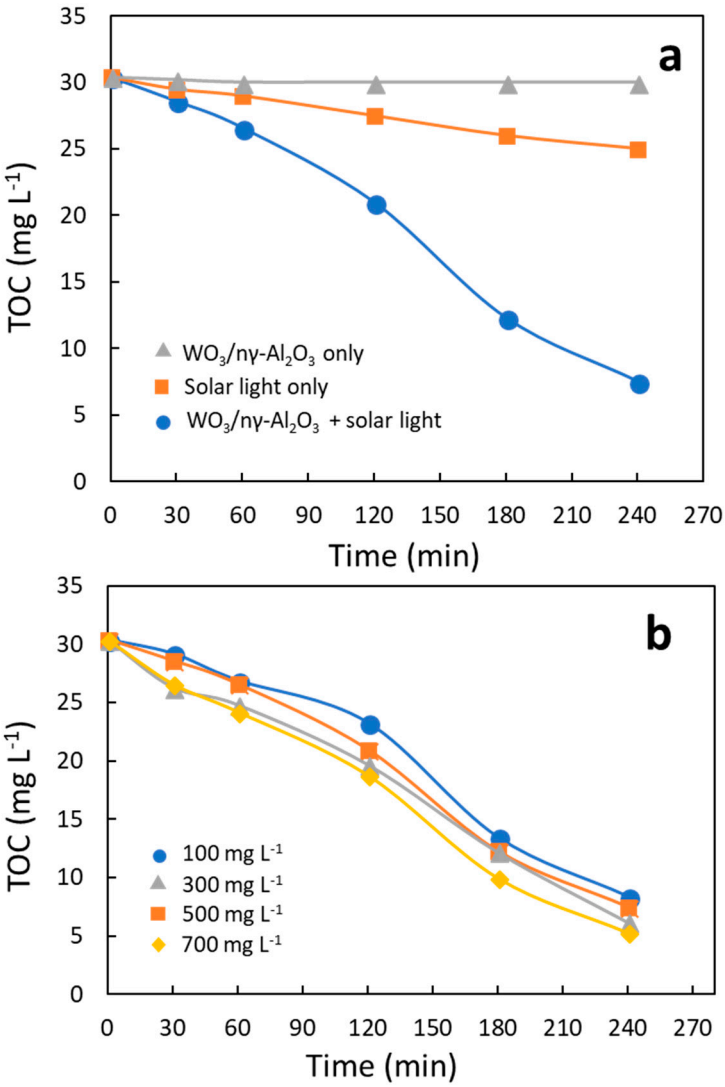

Figure 2. (**a**) Total organic carbon (TOC) reduction of 1,4-D at different reaction conditions and (**b**) the effect of catalyst dose on TOC reduction. $[1,4\text{-D}]_0$ = 50 mg L^{-1}. In (**a**) for both runs in the presence and absence of solar light, [catalyst] = 300 mg L^{-1}.

To check the effect of catalyst dose on mineralization of 1,4-D, various amounts from 100 to 700 mg L^{-1} were tested (Figure 2b). It can be observed that increasing the catalyst dose can improve the treatment efficiency with the final mineralization extent within 67% and 85%. The TOC evolution was fitted to a zero-order kinetic model which has been used in previous photo-oxidation systems [26].

Table 2 collects the corresponding mineralization rate constants with the correlation coefficients (≥ 0.95). It also includes the rate constants obtained using 300 mg L^{-1} of the catalyst alone and using solar light alone. It can be seen that the rate constant of the run using 700 mg L^{-1} of the catalyst reaches up to 0.1059 mg L^{-1} s^{-1}, which is over 4 folds and 81 folds the results achieved when using 300 mg L^{-1} catalyst alone and using solar light alone, respectively. The results confirm the high efficiency of the current WO_3/nγ-Al_2O_3 nano-catalyst for improving the solar-driven photocatalytic systems for the breakdown of 1,4-D.

Table 2. Apparent zero-order kinetic constant rates at different conditions.

Catalysts Dosage (mg L^{-1})	k_{TOC} (mg L^{-1} s^{-1})	R^2
700	0.1059	0.99
500	0.0990	0.99
300	0.0971	0.98
100	0.0927	0.97
300 mg L^{-1}catalyst only	0.0227	0.99
Solar light only	0.0013	0.95

2.3. Oxidation State and Formation of Short-Chain Acids

The mean oxidation state carbon (MOSC) of a solution provides an overall oxidation state of all the compounds in the solution in terms of their averaged MOSC values [50]. MOSC value can be calculated considering both chemical oxidation demand (COD) and TOC via the following equation (Equation (1)).

$$\mathrm{MOSC} = 4 - 1.5\frac{\mathrm{COD}}{\mathrm{TOC}} \quad (1)$$

A higher MOSC value indicates a higher oxidation state, whereas negative ones stand for a higher potential for further oxidation of the compounds in the solution. A previous study reported that the MOSC values of a chemical industrial wastewater containing 1,4-D were within the interval of [4,−4] and 1,4-D had an MOSC value of around 1 [36].

In the current study, to better reveal the oxidation state of the effluent during the course of the reaction, the evolution of solution MOSC was followed and the corresponding results are included in Figure 3a. As can be observed in the figure, the MOSC value of the solution increases from around 1.3 to approximately 3 after 4 h of reaction. This trend is in agreement with a previous work [36]. Extension of reaction time can hardly increase the MOSC value, indicating that the solution reaches a relatively stable oxidation state in the current photocatalytic system.

Some short-chain organic acids were formed after 4 h, including acetic, formic, and fumaric ones (Figure 3b). Among them, acetic acid shows the highest concentration. These short-chain acids have been frequently reported as the final oxidation byproducts in advanced oxidation systems with low ecotoxicity [16,18,51]. It can be concluded that the high MOSC value after reaction must be associated with the formation of these reaction byproducts.

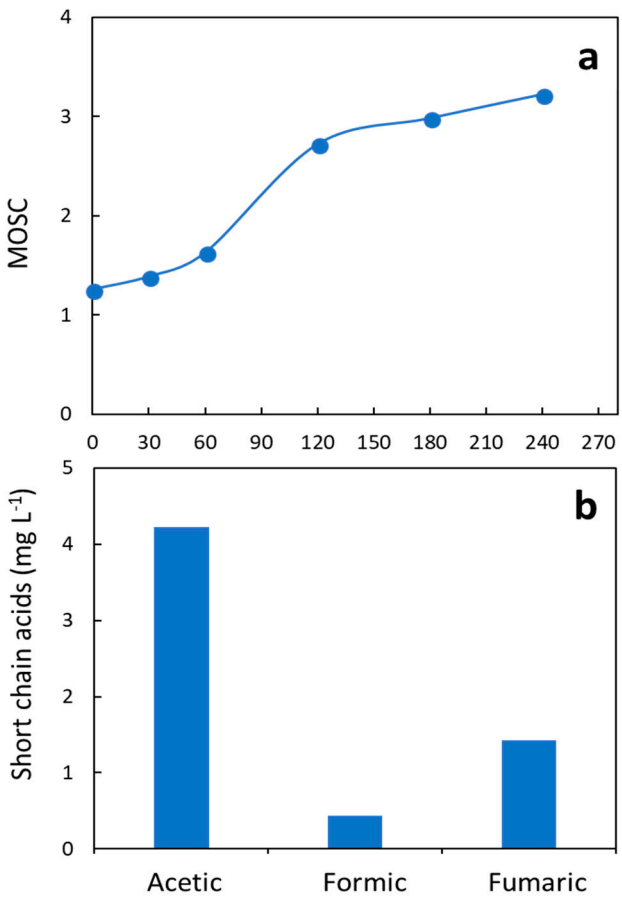

Figure 3. (**a**) Evolution of the mean oxidation state carbon (MOSC) values of 1,4-D aqueous solution during the solar-driven catalytic oxidation and (**b**) the amounts of short-chain acids formed after 4 h of reaction. $[1,4\text{-D}]_0$ = 50 mg L^{-1}; [catalyst] = 300 mg L^{-1}.

2.4. Reusability of the Catalyst

Reusability is an important factor impacting on the potential for practical application of a photocatalyst. In that respect, 300 mg L^{-1} catalyst was added to the system to lead the solar-driven decomposition of 1,4-D for 4 h. Then, the catalyst was separated and dried at 60 °C after reaction, and the same amount of 1,4-D was added again to repeat the reaction. As is shown in Figure 4, a TOC removal of 72.1% is achieved after 7 times of reuse of the catalyst, showing fairly desirable reusability. The slight decline of mineralization extent may be due to the inactivation of the catalyst by adsorption of some reaction byproducts on the active sites.

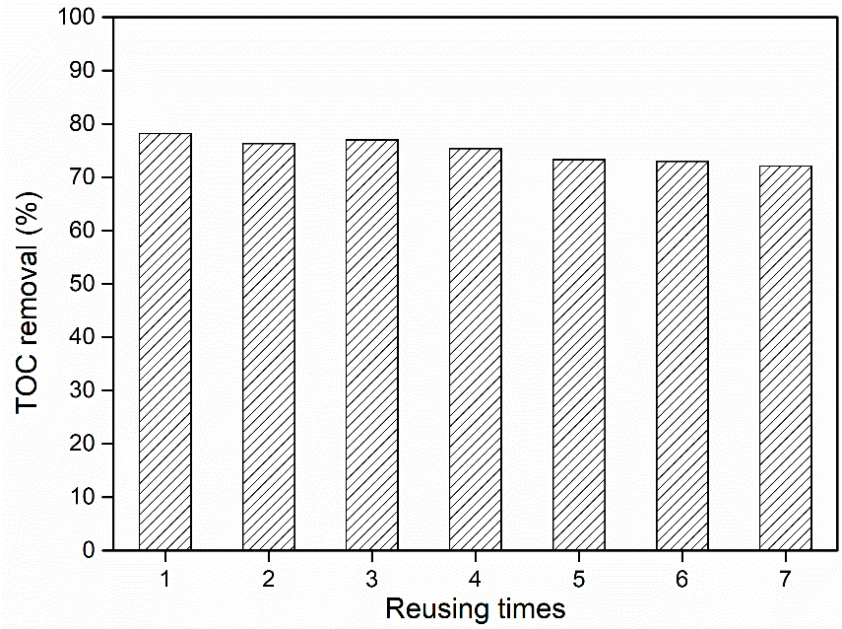

Figure 4. TOC removal of 1,4-D after reuse. $[1,4\text{-D}]_0$ = 50 mg L^{-1}; [catalyst] = 300 mg L^{-1}; reaction time = 4 h.

2.5. Postulation of Photocatalytic Mechanisms

The results so far prove that the current WO_3/nγ-Al_2O_3-based photocatalytic system can effectively remove 1,4-D and the byproducts include some short-chain organic acids. $HO^{\bullet}$ and $O_2^{\bullet-}/HO_2^{\bullet}$ radicals must be responsible for the high efficiency of the current system. These reactive free radicals can be generated through the following scheme: the photon from solar light with certain energy excites the electrons, causing them to transit from the valence band (VB) to the conduction band (CB) and thus, holes are formed on VB. The electron-hole pairs can further excite the dissolved oxygen and water to form ROS (Figure 5). The electrons have a strong reducing ability and can promote the formation of $O_2^{\bullet-}/HO_2^{\bullet}$ radicals from dissolved oxygen. In the meantime, the holes act as positions with high oxidation ability and thus tend to take electrons from water molecules to generate $HO^{\bullet}$ radicals. In addition, the combination of excessive $HO^{\bullet}$ radicals may occur to further form hydrogen peroxide (H_2O_2) [34,52–54]. The above mechanisms enable the current system for the efficient mineralization of the target pollutant 1,4-D in the absence of oxidant (Figure 5).

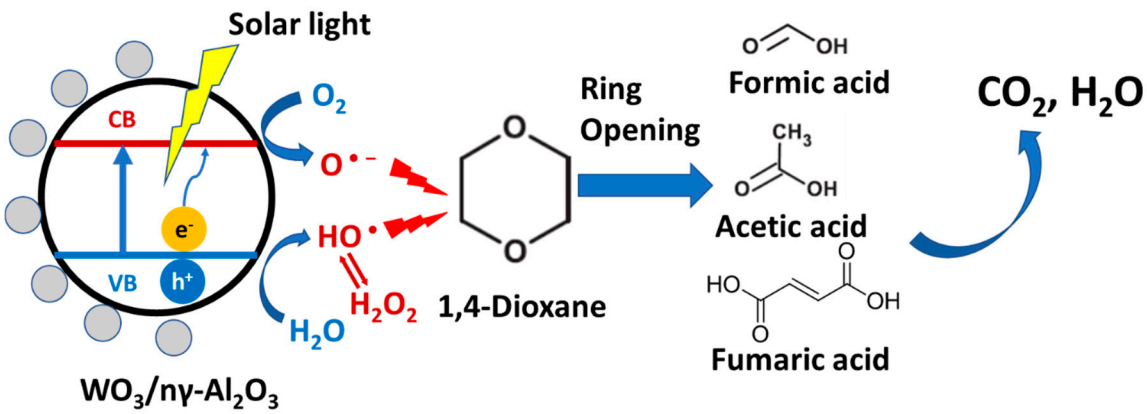

Figure 5. Mechanisms of the degradation of 1,4-D in the current WO_3/nγ-Al_2O_3-based photocatalytic system.

3. Materials and Methods

3.1. Materials

$Na_2WO_4 \cdot 2H_2O$ was purchased from Sigma-Aldrich company, St. Louis, MO, USA. 1,4-D, nano-size γ-Al_2O_3 (nγ-Al_2O_3, diameter < 20 nm) and other reagents were supplied by Aladdin Reagent company, Shanghai, China. All the reagents were of AR grade and used without further purification. Ultrapure water was used throughout the experiments.

The WO_3/nγ-Al_2O_3 catalyst was prepared by incipient wetness impregnation. $Na_2WO_4 \cdot 2H_2O$ (0.08 M) was added drop by drop onto nγ-Al_2O_3 to adjust W load to achieve nominal 5% (*w*/*w*). The impregnated nγ-Al_2O_3 was shaken at room temperature at 60 rpm for 2 h and then dried at 60 °C for 12 h. After that, the sample was calcinated at 300 °C with a heating rate of 4.5 °C min^{-1} from room temperature. The total calcination time was 8 h.

3.2. Characterization of the Catalyst

Surface morphology of the catalyst was observed using SEM (Zeiss Merlin VP Compact, Oberkochen, Germany).

XPS (PHI Quantera SXM, produced by ULVAC-PHI, Chigasaki, Japan) was used to analyze the components on the surface of the catalyst. An Al-Kα X-radiation source was used with a vacuum in the analysis chamber lower than 1.0×10^{-7} Pa. The X-ray beam spot size was 200 μm at an incident angle of 45° with pass energy of 55 eV and step length of 0.1 eV. XPS profiles of W 4f, O 1s and Al 2p were recorded and fitted using XPS Peak 4.1 software.

Quantitative analysis of the compounds on the catalyst surface was conducted using XRF (Shimadzu XRF-1800 SEQUENTIAL, Kyoto, Japan). Based on the protocol, the weight percentage of each compound was presented.

3.3. Solar-Driven Photocatalytic Processes

The solar-driven photocatalytic experiments were conducted in cylinder quartz reactors with a diameter of 6 cm and a height of 7 cm, which were placed in a solar simulator. For a typical run, 100 mL 1,4-D (50 mg L^{-1}) and certain amount of catalyst (100 to 700 mg L^{-1}) were added in the reactor with magnetic stirring at 200 rpm. Then, the lamp was turned on to start the reaction. The light source was a Xe lamp with an irradiation intensity of 40 mW cm^{-2}. The spectrum of the light source is in the range of 190–1100 nm with peaks at 436 nm and 546 nm. The initial pH value of the 1,4-D solution was around 6.8 and not adjusted during the reaction. Solution temperature was controlled by water circulation (< 40 °C after 4 h of reaction), during which no obvious evaporation was observed.

3.4. Analytical Methods

TOC of solution was measured using a TOC analyzer (Shimadzu, model 5000A, Kyoto, Japan). COD was determined by a Hach COD reactor (DRB200, Hach, Loveland, CO, USA) equipped with a spectrophotometer. Organic short-chain acids were measured by an ionic chromatography (IC) equipped with a conductivity detector (Thermo ICS5000+, Waltham, MA, USA). 3.2 mM Na_2CO_3 and 1mM of $NaHCO_3$ were used as mobile phases at pumping rate of 0.7 mL min^{-1}.

4. Conclusions

The current work reports an oxidant-free solar-driven photocatalytic system for the breakdown of 1,4-D based on a homemade WO_3/nγ-Al_2O_3 nano-catalyst. More than 75% mineralization extent can be achieved using 300 mg L^{-1} catalyst at solar light intensity of 40 mW m^{-2} after 4 h of irradiation. Increasing the dose of catalyst to 700 mg L^{-1} can improve the TOC removal to 85%. The MOSC values of the solution were followed and it was found that the oxidation state was greatly raised after reaction. The short-chain acids formed during the reaction—including acetic, formic and fumaric acids—were

believed to be associated with the high solution oxidation state. A reusability study indicates that the current catalyst can still be efficient after being reused seven times.

The current work provides a promising approach to eliminate 1,4-D from water for potable reuse. It is not only oxidant-free but can also make use of solar light radiation to lead 1,4-D mineralization. However, it should be noticed that around 20% of organic carbons still remain in the solution after treatment. In that sense, future studies should be conducted to either analyze the composition of these organic carbons or evaluate their ecotoxicity.

Author Contributions: Conceptualization, X.X., S.L. and K.S.; methodology, X.X., S.L., Y.C., X.W., K.S. and Y.W.; software, X.X. and X.W.; validation, X.X.; formal analysis, X.X.; investigation, X.X., S.L., Y.C. and X.W.; resources, Y.W.; data curation, X.X., Y.C. and X.W.; writing—original draft preparation, X.X.; writing—review and editing, X.X., S.L., Y.C., X.W., K.S. and Y.W.; visualization, X.X. and K.S.; supervision, S.L. and Y.W.; project administration, S.L. and Y.W.; funding acquisition, S.L.

Acknowledgments: We are grateful for the support of the National Natural Science Foundation of China (51808312, 51879139), China Postdoctoral Science Foundation (No. 2018M631495), and the National Key Research and Development Program of China for International Science & Innovation Cooperation Major Project between Governments (2016YFE0118800).

Conflicts of Interest: The authors declare no conflict of interest.

References

1. Patton, S.; Romano, M.; Naddeo, V.; Ishida, K.P.; Liu, H. Photolysis of mono- and dichloramines in UV/Hydrogen peroxide: Effects on 1,4-Dioxane removal and relevance in water reuse. *Environ. Sci. Technol.* **2018**, *52*, 11720–11727. [CrossRef] [PubMed]
2. Du, Y.; Wu, Q.Y.; Lv, X.T.; Ye, B.; Zhan, X.M.; Lu, Y.; Hu, H.Y. Electron donating capacity reduction of dissolved organic matter by solar irradiation reduces the cytotoxicity formation potential during wastewater chlorination. *Water Res.* **2018**, *145*, 94–102. [CrossRef] [PubMed]
3. Liu, S.; Che, H.; Smith, K.; Lei, M.; Li, R. Performance evaluation for three pollution detection methods using data from a real contamination accident. *J. Environ. Manage.* **2015**, *161*, 385–391. [CrossRef] [PubMed]
4. Xu, X.; Liu, Y.; Liu, S.; Li, J.; Guo, G.; Smith, K. Real-time detection of potable-reclaimed water pipe cross-connection events by conventional water quality sensors using machine learning methods. *J. Environ. Manag.* **2019**, *238*, 201–209. [CrossRef]
5. Li, W.; Patton, S.; Gleason, J.M.; Mezyk, S.P.; Ishida, K.P.; Liu, H. UV Photolysis of chloramine and persulfate for 1,4-Dioxane removal in reverse-osmosis permeate for potable water reuse. *Environ. Sci. Technol.* **2018**, *52*, 6417–6425. [CrossRef] [PubMed]
6. Cheng, M.; Zeng, G.; Huang, D.; Lai, C.; Liu, Y.; Zhang, C.; Wan, J.; Hu, L.; Zhou, C.; Xiong, W. Efficient degradation of sulfamethazine in simulated and real wastewater at slightly basic pH values using Co-SAM-SCS/H_2O_2 Fenton-like system. *Water Res.* **2018**, *138*, 7–18. [CrossRef] [PubMed]
7. Zhang, T.Y.; Hu, H.Y.; Wu, Y.H.; Zhuang, L.L.; Xu, X.Q.; Wang, X.X.; Dao, G.H. Promising solutions to solve the bottlenecks in the large-scale cultivation of microalgae for biomass/bioenergy production. *Renew. Sust. Energ. Rev.* **2016**, *60*, 1602–1614. [CrossRef]
8. Cheng, M.; Lai, C.; Liu, Y.; Zeng, G.; Huang, D.; Zhang, C.; Qin, L.; Hu, L.; Zhou, C.; Xiong, W. Metal-organic frameworks for highly efficient heterogeneous Fenton-like catalysis. *Coordin. Chem. Rev.* **2018**, *368*, 80–92.
9. Chen, A.; Shang, C.; Shao, J.; Lin, Y.; Luo, S.; Zhang, J.; Huang, H.; Lei, M.; Zeng, Q. Carbon disulfide-modified magnetic ion-imprinted chitosan-Fe(III): A novel adsorbent for simultaneous removal of tetracycline and cadmium. *Carbohyd. Polym.* **2017**, *155*, 19–27. [CrossRef]
10. Warsinger, D.M.; Chakraborty, S.; Tow, E.W.; Plumlee, M.H.; Bellona, C.; Loutatidou, S.; Karimi, L.; Mikelonis, A.M.; Achilli, A.; Ghassemi, A.; et al. A review of polymeric membranes and processes for potable water reuse. *Prog. Poly. Sci.* **2018**, *81*, 209–237. [CrossRef]
11. Tahara, M.; Obama, T.; Ikarashi, Y. Development of analytical method for determination of 1,4-dioxane in cleansing products. *Int. J. Cosmetic Sci.* **2013**, *35*, 575–580. [CrossRef] [PubMed]
12. Guo, P.-y. Determination of dioxane in toiletries by headspace gas chromatography-mass spectrometry. *Deter. Cosm.* **2013**, *36*, 20–22.
13. Guo, W.Q.; Brodowsky, H. Determination of the trace 1,4-dioxane. *Microchem. J.* **2000**, *64*, 173–179. [CrossRef]

14. Nannelli, A.; De Rubertis, A.; Longo, V.; Gervasi, P. Effects of dioxane on cytochrome P450 enzymes in liver, kidney, lung and nasal mucosa of rat. *Arch. Toxicol.* **2005**, *79*, 74–82. [CrossRef] [PubMed]
15. Stickney, J.A.; Sager, S.L.; Clarkson, J.R.; Smith, L.A.; Locey, B.J.; Bock, M.J.; Hartung, R.; Olp, S.F. An updated evaluation of the carcinogenic potential of 1,4-dioxane. *Regul. Toxicol. Pharm.* **2003**, *38*, 183–195. [CrossRef]
16. Xu, X.; Pliego, G.; Garcia-Costa, A.L.; Zazo, J.A.; Liu, S.; Casas, J.A.; Rodriguez, J.J. Cyclohexanoic acid breakdown by two-step persulfate and heterogeneous Fenton-like oxidation. *Appl. Catal. B-Environ.* **2018**, *232*, 429–435. [CrossRef]
17. Xu, X.; Pliego, G.; Zazo, J.A.; Sun, S.; García-Muñoz, P.; He, L.; Casas, J.A.; Rodriguez, J.J. An overview on the application of advanced oxidation processes for the removal of naphthenic acids from water. *Crit. Rev. Environ. Sci. Technol.* **2017**, *47*, 1337–1370. [CrossRef]
18. Munoz, M.; Mora, F.J.; Pedro, Z.M.D.; Alvarez-Torrellas, S.; Casas, J.A.; Rodriguez, J.J. Application of CWPO to the treatment of pharmaceutical emerging pollutants in different water matrices with a ferromagnetic catalyst. *J. Hazard. Mater.* **2017**, *331*, 45–54. [CrossRef] [PubMed]
19. Munoz, M.; de Pedro, Z.M.; Casas, J.A.; Rodriguez, J.J. Preparation of magnetite-based catalysts and their application in heterogeneous Fenton oxidation–a review. *Appl. Catal. B-Environ.* **2015**, *176*, 249–265. [CrossRef]
20. Quintanilla, A.; Casas, J.; Rodriguez, J. Hydrogen peroxide-promoted-CWAO of phenol with activated carbon. *Appl. Catal. B-Environ.* **2010**, *93*, 339–345. [CrossRef]
21. Quintanilla, A.; Fraile, A.; Casas, J.; Rodríguez, J. Phenol oxidation by a sequential CWPO–CWAO treatment with a Fe/AC catalyst. *J. Hazard. Mater.* **2007**, *146*, 582–588. [CrossRef] [PubMed]
22. Anipsitakis, G.P.; Dionysiou, D.D.; Gonzalez, M.A. Cobalt-mediated activation of peroxymonosulfate and sulfate radical attack on phenolic compounds. Implications of chloride ions. *Environ. Sci. Technol.* **2006**, *40*, 1000–1007. [CrossRef] [PubMed]
23. Anipsitakis, G.P.; Dionysiou, D.D. Radical generation by the interaction of transition metals with common oxidants. *Environ. Sci. Technol.* **2004**, *38*, 3705–3712. [CrossRef]
24. Xu, X.; Pliego, G.; Zazo, J.A.; Casas, J.A.; Rodriguez, J.J. Mineralization of naphtenic acids with thermally-activated persulfate: The important role of oxygen. *J. Hazard. Mater.* **2016**, *318*, 355–362. [CrossRef] [PubMed]
25. Pliego, G.; Zazo, J.A.; Garcia-Muñoz, P.; Munoz, M.; Casas, J.A.; Rodriguez, J.J. Trends in the intensification of the Fenton process for wastewater treatment: An overview. *Crit. Rev. Environ. Sci. Technol.* **2015**, *45*, 2611–2692. [CrossRef]
26. García-Muñoz, P.; Pliego, G.; Zazo, J.; Barbero, B.; Bahamonde, A.; Casas, J. Modified ilmenite as catalyst for CWPO-Photoassisted process under LED Light. *Chem. Eng. J.* **2017**, *318*, 89–94.
27. Wols, B.A.; Hofman-Caris, C.H.M. Review of photochemical reaction constants of organic micropollutants required for UV advanced oxidation processes in water. *Water Res.* **2012**, *46*, 2815–2827. [CrossRef] [PubMed]
28. Barndok, H.; Hermosilla, D.; Negro, C.; Blanco, A. Comparison and Predesign Cost Assessment of different advanced oxidation processes for the treatment of 1,4-Dioxane-containing wastewater from the chemical industry. *ACS Sustain. Chem. Eng.* **2018**, *6*, 5888–5894. [CrossRef]
29. Barndok, H.; Merayo, N.; Blanco, L.; Hermosilla, D.; Blanco, A. Application of on-line FTIR methodology to study the mechanisms of heterogeneous advanced oxidation processes. *Appl. Catal. B-Environ.* **2016**, *185*, 344–352. [CrossRef]
30. Gomez-Aviles, A.; Penas-Garzon, M.; Bedia, J.; Rodriguez, J.J.; Belver, C. C-modified TiO2 using lignin as carbon precursor for the solar photocatalytic degradation of acetaminophen. *Chem. Eng. J.* **2019**, *358*, 1574–1582. [CrossRef]
31. Belver, C.; Bedia, J.; Rodriguez, J.J. Titania-clay heterostructures with solar photocatalytic applications. *Appl. Catal. B-Environ.* **2015**, *176–177*, 278–287. [CrossRef]
32. Belver, C.; Han, C.; Rodriguez, J.J.; Dionysiou, D.D. Innovative W-doped titanium dioxide anchored on clay for photocatalytic removal of atrazine. *Catal. Today* **2017**, *280*, 21–28. [CrossRef]
33. Zhang, C.; Li, Y.; Shuai, D.; Shen, Y.; Xiong, W.; Wang, L. Graphitic carbon nitride (g-C3N4)-based photocatalysts for water disinfection and microbial control: A review. *Chemosphere* **2019**, *214*, 462–479. [CrossRef] [PubMed]
34. Mazierski, P.; Mikolajczyk, A.; Bajorowicz, B.; Malankowska, A.; Zaleska-Medynska, A.; Nadolna, J. The role of lanthanides in TiO_2-based photocatalysis: A review. *Appl. Catal. B-Environ.* **2018**, *233*, 301–317. [CrossRef]

35. Hill, R.R.; Jeffs, G.E.; Roberts, D.R. Photocatalytic degradation of 1,4-Dioxane in aqueous solution. *J. Photoch. Photobio. A* **1997**, *108*, 55–58. [CrossRef]
36. Barndok, H.; Blanco, L.; Hermosilla, D.; Blanco, A. Heterogeneous photo-Fenton processes using zero valent iron microspheres for the treatment of wastewaters contaminated with 1,4-Dioxane. *Chem. Eng. J.* **2016**, *284*, 112–121. [CrossRef]
37. Lee, K.-C.; Beak, H.-J.; Choo, K.-H. Membrane photoreactor treatment of 1,4-Dioxane-containing textile wastewater effluent: Performance, modeling, and fouling control. *Water Res.* **2015**, *86*, 58–65. [CrossRef]
38. Tian, J.; Sang, Y.; Yu, G.; Jiang, H.; Mu, X.; Liu, H. A Bi_2WO_6-Based hybrid photocatalyst with broad spectrum photocatalytic properties under UV, visible, and near-infrared irradiation. *Adv. Mater.* **2013**, *25*, 5075–5080. [CrossRef]
39. Ribeiro, A.R.; Nunes, O.C.; Pereira, M.F.R.; Silva, A.M.T. An overview on the advanced oxidation processes applied for the treatment of water pollutants defined in the recently launched Directive 2013/39/EU. *Environ. Int.* **2015**, *75*, 33–51. [CrossRef]
40. Ravelli, D.; Protti, S.; Fagnoni, M. Decatungstate anion for photocatalyzed "window ledge" reactions. *Accounts Chem. Res.* **2016**, *49*, 2232–2242. [CrossRef]
41. El-Sheikh, S.M.; Rashad, M.M. Novel Synthesis of Cobalt Nickel Tungstate Nanopowders and its photocatalytic application. *J. Clust. Sci.* **2015**, *26*, 743–757. [CrossRef]
42. Huang, Z.F.; Song, J.; Pan, L.; Zhang, X.; Wang, L.; Zou, J.J. Tungsten oxides for photocatalysis, electrochemistry, and phototherapy. *Adv. Mater.* **2015**, *27*, 5309–5327. [CrossRef] [PubMed]
43. Visa, M.; Bogatu, C.; Duta, A. Tungsten oxide–fly ash oxide composites in adsorption and photocatalysis. *J. Hazard. Mater.* **2015**, *289*, 244–256. [CrossRef]
44. Xu, H.; Yu, T.; Liu, J. Photo-degradation of Acid Yellow 11 in aqueous on nano-ZnO/Bentonite under ultraviolet and visible light irradiation. *Mater. Lett.* **2014**, *117*, 263–265. [CrossRef]
45. Barrault, J.; Boulinguiez, M.; Forquy, C.; Maurel, R. Synthesis of methyl mercaptan from carbon oxides and H_2S with tungsten—alumina catalysts. *Appl. Catal.* **1987**, *33*, 309–330. [CrossRef]
46. Halada, G.; Clayton, C. Comparison of Mo–N and W–N synergism during passivation of stainless steel through X-ray photoelectron spectroscopy and electrochemical analysis. *J. Vac. Sci. Technol. A* **1993**, *11*, 2342–2347. [CrossRef]
47. Kerkhof, F.P.J.M.; Moulijn, J.A.; Heeres, A. The XPS spectra of the metathesis catalyst tungsten oxide on silica gel. *J. Electron. Spectrosc.* **1978**, *14*, 453–466. [CrossRef]
48. Carley, A.; Roberts, M. An X-ray photoelectron spectroscopic study of the interaction of oxygen and nitric oxide with aluminium. *P. Roy. Soc. Lond. A* **1978**, *363*, 403–424. [CrossRef]
49. Ealet, B.; Elyakhloufi, M.H.; Gillet, E.; Ricci, M. Electronic and crystallographic structure of γ-alumina thin films, Thin Solid Films, 1994, 250, 92–100. *Thin Solid Films* **1994**, *250*, 92–100. [CrossRef]
50. Vogel, F.; Harf, J.; Hug, A.; von Rohr, P.R. The mean oxidation number of carbon (MOC)—A useful concept for describing oxidation processes. *Water Res.* **2000**, *34*, 2689–2702. [CrossRef]
51. Peng, Y.; Fu, D.; Liu, R.; Zhang, F.; Xue, X.; Xu, Q.; Liang, X. $NaNO_2/FeCl_3$ dioxygen recyclable activator: An efficient approach to active oxygen species for degradation of a broad range of organic dye pollutants in water. *Appl. Catal. B-Environ.* **2008**, *79*, 163–170. [CrossRef]
52. Wang, C.; Ao, Y.; Wang, P.; Hou, J.; Qian, J. Preparation, characterization and photocatalytic activity of the neodymium-doped TiO_2 hollow spheres. *Appl. Sur. Sci.* **2010**, *257*, 227–231. [CrossRef]
53. Mehrvar, M.; Anderson, W.A.; Moo-Young, M. Photocatalytic degradation of aqueous tetrahydrofuran, 1,4-dioxane, and their mixture with TiO_2. *Inter. J. Photoenerg.* **2000**, *2*, 67–80. [CrossRef]
54. Asghar, A.; Abdul Raman, A.A.; Wan Daud, W.M.A. Advanced oxidation processes for in-situ production of hydrogen peroxide/hydroxyl radical for textile wastewater treatment: A review. *J. Clean. Prod.* **2015**, *87*, 826–838. [CrossRef]